Nanoscale Advances

ROYAL SOCIETY OF CHEMISTRY

PAPER

View Article Online
View Journal

Cite this: DOI: 10.1039/d6na00100a

A comprehensive design framework for all-dielectric metasurfaces by harnessing the interplay of controlled multiple multipole excitation, Rayleigh anomaly, Mie and lattice resonances

Tummaluru Khadar Basha,[a] Faraz A. Inam[b] and Junaid Masud Laskar *[a]

Dielectric metasurfaces have emerged as promising candidates for controlling electromagnetic (EM) multipoles, crucial for precise manipulation of associated light–matter interactions, particularly for multifunctionality in photonics technologies spanning across structural scales and the EM spectrum. Each multipole with a given nature (electric-E, magnetic-H) and order (dipole-D, quadrupole-Q) has specific functionality with implications on resonance types (fundamental as well as collective), their coupling and hybridization. By using geometrical dimensions as the primary design parameters, only a few multipoles have been reported to be excited simultaneously. Moreover, an understanding of the relationship among meta-atom Mie resonances, lattice periodicity, and lattice resonances is still lacking. The local field distribution due to spatial hybridization with neighboring meta-atoms is also unknown for finite metasurfaces. We have developed a comprehensive design framework to maximize resonance strength by controlled multipole excitation, overlap, and coupling among different resonance types, including Mie, lattice, Rayleigh anomaly, and local fields in metasurfaces, using numerical simulations. The simultaneous spectral overlap of four multipoles (ED, MD, EQ, and MQ) is demonstrated when the meta-atom height exceeds the excitation wavelength. As periodicity matches both the Mie and Rayleigh anomaly wavelengths, the resulting metasurface resonance attains a high Q factor, attributed to maximum coupling of Mie and lattice resonances. Spatial field hybridization due to the specific arrangement of neighboring meta-atoms, depending on array size, results in asymmetric local field distributions in finite metasurfaces, crucial for real-world implementations. Our findings reveal governing principles linking controlled multipole excitation dynamics, the influence of coupling among different resonance types on the resultant resonances, and local field distributions relevant to multifunctional metasurface photonics and integrated quantum technologies.

Received 9th February 2026
Accepted 28th April 2026

DOI: 10.1039/d6na00100a

rsc.li/nanoscale-advances

Introduction

Resonances are ubiquitous in nature, creating striking visual effects, as seen in opal gemstones,[1] beetles,[2] and butterfly wings,[3] particularly in the context of light–matter interactions,[4] arising in systems where an electromagnetic (EM) wave interferes with geometry to create a strong EM field enhancement at specific frequencies or wavelengths.[5] Resonant systems span from simple geometric cavities, such as antennas,[6] meta-atoms,[5,7–9] Fabry–Perot cavities,[10] ring resonators,[11] and whispering-gallery-mode resonators,[12] to complex periodic structures, such as photonic crystals[13] and metasurfaces,[5,8,9,14–16] by making use of different mechanisms, including Mie resonances,[5,9,14–17] plasmonic resonances,[7] guided-mode resonances,[18,19] Fano resonances,[20] lattice resonances,[21–24] and bound states in the continuum (BICs).[25]

In the dielectric meta-atom, a basic resonant photonic system, having its dimension on the order of the excitation EM wavelength and matching the wavelength of EM multipole oscillations of different nature (electric and magnetic) and order (dipoles and quadrupoles), resonant excitation of multipoles takes place, known as Mie resonances (λ_{Mie}).[9,14–17,26,27] Computational design and experimental investigations of meta-atoms of different shapes are carried out with a focus on resonant multipole excitation, amplitude enhancement, spectral tuning, and the overlap of multiple resonance peaks. However, despite the significant effort in the last decade, multipole overlap has been limited only to electric multipoles of two different orders, ED, EQ, and lower-order MD, leaving out MQ, which is crucial to enhance the magnetic emitter emissivity and nonlinear optical signals.[9,14–16,26]

[a]Nanophotonics and Quantum Meta-Optics Group, Center for Nanophotonics, Department of Physics and Nanotechnology, SRM Institute of Science and Technology, Kattankulathur, Chennai, Tamil Nadu, PIN-603203, India. E-mail: junaidmb@srmist.edu.in

[b]Department of Physics, Aligarh Muslim University, Aligarh, Uttar Pradesh, PIN-202002, India

It still remains a challenge to simultaneously harness four multipoles of different nature and order, ED, MD, EQ, and MQ, through their overlap as well as their field enhancement to nearly equal amplitude at a fixed geometrical dimension.

A 2D crystal lattice structure, with meta-atoms acting as the crystal basis located at lattice sites, is known as the metasurface.[5,7,15,16,28,29] Metasurface is one of the most prominent resonant photonic systems, which allows to realize a high Q factor, a characterizing parameter of a resonator defined as the ratio of energy stored to energy lost per radiation cycle.[30] The metasurface lattice resonance ($\lambda_{MS\text{-}Res}$), manifested as peaks in the EM spectra, originates from the coupling between Mie resonances ($\lambda_{Mie} \equiv \lambda_{MA\text{-}Res}$) of each meta-atom and the lattice periodicity (P_{MS}), *i.e.*, meta-atom spacing-dependent lattice resonances ($\lambda_{LS\text{-}Res}$).[7,15,16,21,22,30–33] The interaction of EM waves with a periodic lattice structure, not necessarily having resonant meta-atoms as the basis, results in a diffraction pattern, which is the appearance of alternating intensity maxima and minima, also known as lattice resonances or diffraction orders, whose angular positions can be accurately estimated by diffraction theory.[34] Interestingly, as an anomaly to the diffraction theory, rapid variations in expected intensities corresponding to different diffraction orders, known as the Rayleigh anomaly (RA) at specific wavelengths (λ_{RA}) depending on the lattice periodicity (P_{MS}), are observed in diffraction gratings, the periodic lattice structures of both metals and dielectrics.[19,31,34–36] By varying the values of the metasurface P_{MS} around the corresponding λ_{RA} values, along two different horizontal directions of a metasurface, enhancement of lattice resonances (LR) due to combinations of two multipoles of different nature and order—(a) ED-LR[15,23,30,37] and MD-LR,[15,23,30,32,37,38] (b) MD-LR[15,23,30,32,37,38] and EQ-LR[15,23,30,39–41]—as well as due to single multipoles—(a) ED-LR[30,37] and (b) MQ-LR[39,42]—are shown previously. However, achieving an extremely high Q factor in a metasurface requires the simultaneous resonant excitation and spectral overlap of multiple multipoles of different nature and order. In this regard, a larger range of meta-atom spacing, the lattice periodicity (P_{MS}) around the corresponding λ_{RA} values, need to be explored. Therefore, an investigation of the role of P_{MS} on the interplay among different natures and orders of multipoles, as well as resonance types, (i) meta-atom Mie resonances ($\lambda_{MA\text{-}Res}$), (ii) metasurface lattice resonances ($\lambda_{MS\text{-}Res}$), and (iii) Rayleigh anomaly wavelengths (λ_{RA}), is essential across a larger range of lattice periodicities (P_{MS}), spanning four regimes: (a) small ($P_{MS} < \lambda_{MA\text{-}Res}$), (b) intermediate ($P_{MS} \leq \lambda_{MA\text{-}Res}$), (c) comparable ($P_{MS} \sim \lambda_{MA\text{-}Res}$) and (d) large ($P_{MS} > \lambda_{MA\text{-}Res}$). It will provide deeper insight.

Metasurfaces used in real-world applications are constituted by a finite number of meta-atoms. However, investigations carried out until now have mostly focused on computational design simulations of infinite metasurfaces, in order to reduce computational cost by modelling only a unit cell and applying periodic boundary conditions.[43] In infinite metasurface numerical simulations, the amplitude enhancement of resonantly excited EM multipoles and the role of their coupling on resultant high-Q-factor resonances in the EM spectra can only be computed.[33,44–47] The knowledge of local EM field distributions around specific locations of each meta-atom in the near-field, particularly the influence of neighboring meta-atoms and their spatial arrangement, is hardly addressed in infinite metasurface numerical computations.

In this paper, by making use of finite element method-based numerical computational simulations, we have developed a comprehensive conceptual design framework to maximize dielectric metasurface resonances and near-field distributions

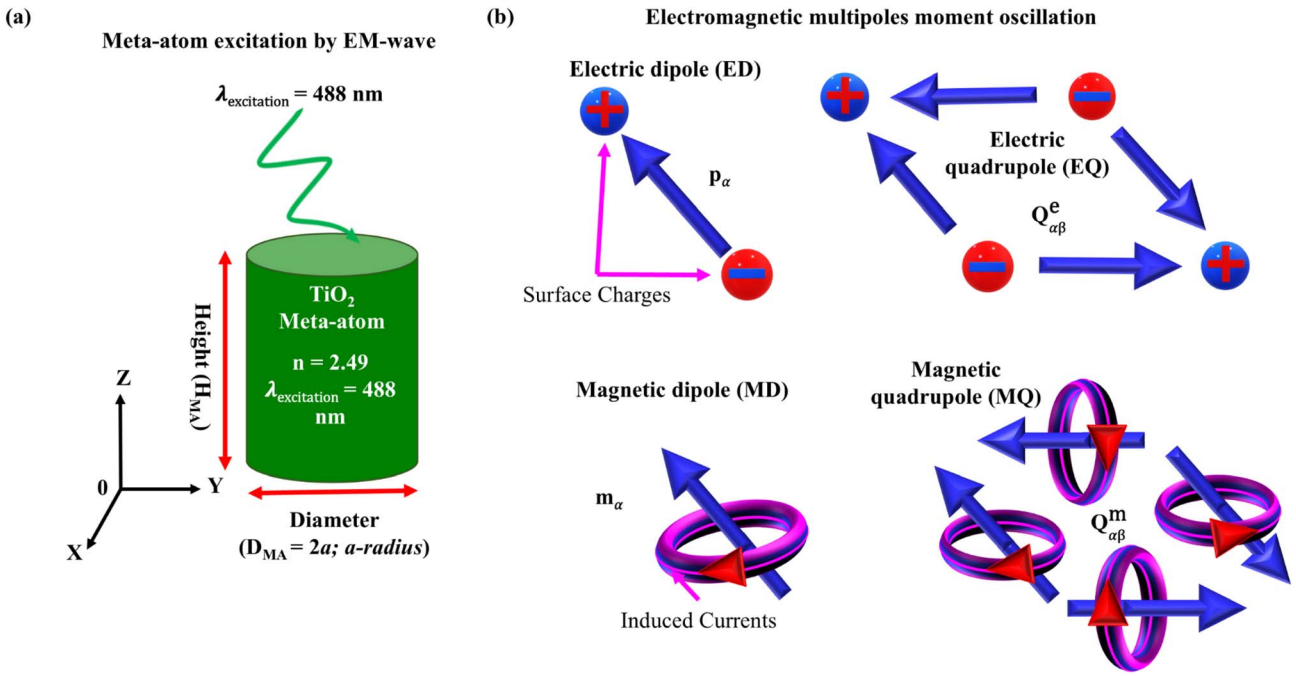

Fig. 1 (a) Schematic of EM wave excitation of a meta-atom (TiO_2, n_{TiO_2} = 2.49@$\lambda_{excitation}$ = 488 nm) and (b) EM multipole moment dipole oscillation configurations.

at sub-meta-atom scale by harnessing the simultaneous resonant excitation of EM multipoles of different nature and order corresponding to different resonance types across hierarchical scales. Particularly, the interplay among crucial control parameters, including meta-atom geometrical dimensions (diameter, D_{MA}, and height, H_{MA}), metasurface lattice periodicity with regard to the Rayleigh anomaly wavelength (λ_{RA}), and number of meta-atoms (N_{MS}) on meta-atom Mie resonances ($\lambda_{MA\text{-}Res}$), their coupling with diffraction lattice resonances and EM field hybridization due to the spatial arrangement of neighboring meta-atoms, is investigated systematically. Deeper insight into these studies is crucial for real-world metasurface applications, including Huygens metasurface,[48] cavity-free quantum electrodynamics-based resonant integrated photonic devices,[46] integration with quantum light sources,[49] Raman emitters,[50] low-threshold nano-lasers,[51] and quantum sensing.[52]

Numerical computation (finite element method: FEM) of scattering cross-section (C_{sca}) and EM field distribution of both finite and infinite metasurfaces

The numerical computational simulations of EM scattering cross-sections (C_{sca}) and EM field distributions for (a) a cylindrical dielectric (TiO_2) meta-atom, (b) an infinite metasurface on applying periodic boundary conditions (PBC) and (c) metasurface with a finite number of meta-atoms are performed using the finite element method (FEM) within the EM wave frequency domain of wave optics module [COMSOL multiphysics software (version 6.2)]. The EM wave excitation of the meta-atom and metasurface are conducted along the Z-direction (Fig. 1a), with air ($n_{air} = 1$) as the surrounding medium. Previously reported values of the refractive indices are used for both the meta-atom (TiO_2, $n_{TiO_2} = 2.49@\lambda_{excitation} = 488$ nm)[53] as well as for the substrate (Si, $n_{Si} = 3.65@\lambda_{excitation} = 488$ nm).[54] In order to minimize undesired reflections of scattered EM waves, a perfectly matched layer (PML), serving as an artificial absorbing layer, is used at the interface boundary with the surrounding air medium. The size of the mesh elements is varied from 2 nm to ($\lambda_{excitation}/6$) to ensure accurate computation of the EM field distribution. The induced current densities (J_ω)[55] (eqn (3) in the SI) and the corresponding EM multipole moments of different orders (eqn (4)–(7) in the SI) are computed for each element corresponding to a certain value of spatial position vector (r) [Fig. 1].

Results and discussion

The effects of the geometric parameters, including the meta-atom height (H_{MA}), metasurface array periodicity (P_{Ms}), and the number of meta-atoms (N_{Ms}), on the C_{sca}^{total} and on the scattering cross-sections corresponding to multipole moments, ED, MD, EQ, MQ, are investigated, particularly in the Mie regime, $H_{MA} \sim P_{Ms} \sim \lambda_{excitation}$.

Height of meta-atom dictates the overlap of multiple EM multipoles: the Mie resonance

With an increase in meta-atom height (H_{MA}), shifts in the multipole peaks and their overlap in the EM spectra are observed under the excitation by the EM wave ($\lambda_{excitation} = 488$ nm), as shown in Fig. 2. The total scattering cross-section (C_{sca}^{total}) is shown as a function of the size parameter $\left(ka = \frac{2\pi na}{\lambda_{excitation}}\right)$.[56] The spectral peaks physically signify the decomposition of Mie resonances into multipoles of different nature (electric and magnetic) and orders (dipoles and quadrupoles).[56–58] Lower-order multipoles—ED and MD—can be excited at shorter meta-atom heights ($H_{MA} < \lambda_{excitation}$).[57,58] With an increase in the height ($H_{MA} \sim \lambda_{excitation}$, Fig. 2c), the amplitude of the lower-order resonance modes, ED and MD, do not vary significantly. However, their spectral peak widths decrease, signifying an enhancement in the Q factor of the corresponding mode. Meta-atoms with shorter height ($H_{MA} < \lambda_{excitation}$) [Fig. 2a and b] are unable to support higher-order multipoles, such as EQ and MQ.[40,59]

By significantly increasing meta-atom height ($H_{MA} > \lambda_{excitation}$, Fig. 2d), two key aspects are observed with regard to the higher-order multipoles (EQ and MQ): (a) an enhancement in peak amplitude and (b) spectral peak shift towards lower size parameter values ($ka = 0.77$). This red spectral shift leads to a larger degree of overlap between higher-order multiples (EQ and MQ) and the lower ones (ED and MD), both in terms of spectral peak position and amplitude [Fig. 2d].[57,58] The red shift of spectral peak as a function of increasing height (H_{MA}) is also observed in dielectric Si meta-atoms, unlike the blue-shift observed for plasmonic meta-atoms, attributed to the increased restoring force between positively charged atomic nuclei and the displaced negatively charged electron cloud, upon being excited by an EM wave.[58]

Physically, higher-order multipoles in dielectrics (*e.g.*, TiO_2 and Si), particularly the quadrupole moments (EQ and MQ), can be considered a couple of anti-parallel dipole moments [Fig. 1b], which requires sufficiently large enough physical space along a specific direction, which in this case is the Z axis, *i.e.*, the meta-atom height H_{MA} direction, so that a quadrupolar arrangement of field distribution can be accommodated within the meta-atom.[59] Moreover, increasing the meta-atom height H_{MA}, resulting in larger values of the position vector (r) (Fig. 1), satisfies the conditions for the Bessel functions of the first kind with higher orders (second- and third-order terms, j_2 and j_3), $\frac{j_1(kr)}{kr}$, together with the inverse power law $\left(\frac{1}{r^2} \text{ and } \frac{1}{r^3}\right)$, so that maximum peaks are allowed to form, acting as higher-order modes, EQ and MQ (eqn (6) and (7), SI).[55] Despite the overlap of all multipoles (ED, MD, EQ, and MQ) at a size parameter of $ka = 0.77$, designated as Mie mode-1, a new mode-2 also gets developed at a larger of $ka = 1.2$, where both enhancement and overlap of multipoles take place, for $H_{MA} > \lambda_{excitation}$, as shown in Fig. 2d. The enhancement of Mie multipole resonance modes and their overlap signify that, for a meta-atom with a given refractive index (n), the geometric parameter—the meta-atom height H_{MA}—normalized with regard to the excitation wavelength $\lambda_{excitation}$ can be used as the primary design control parameter for the efficient design of

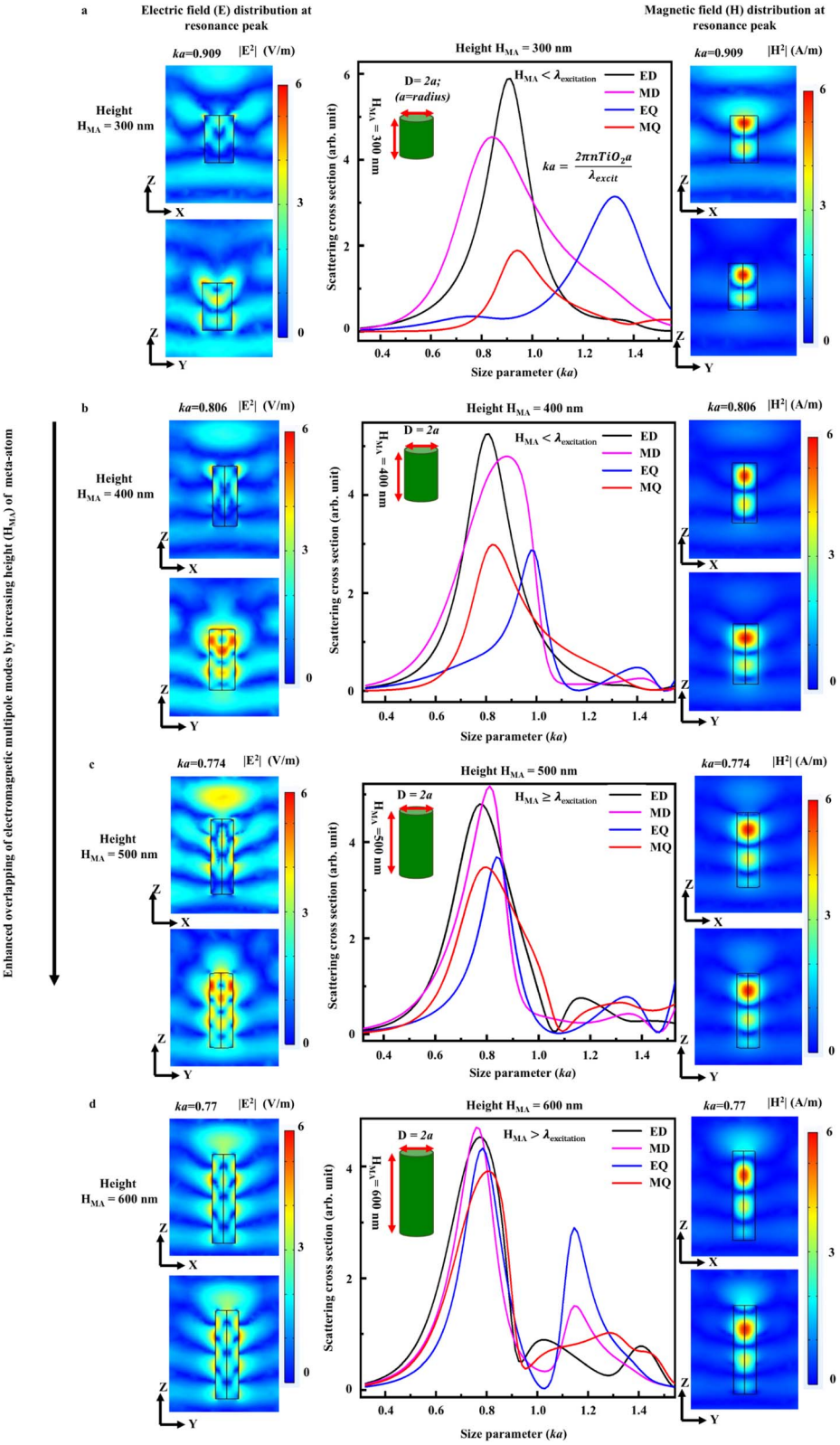

Fig. 2 Scattering cross-section $C_{sca\ (center\ column)}^{total}$, electric (left column) and magnetic field (right column) distributions of EM multipoles for different meta-atom heights (H_{MA}) in the Mie regime ($H_{MA} \sim \lambda_{excitation}$) (a) $H_{MA} = 300$ nm, (b) $H_{MA} = 400$ nm, (c) $H_{MA} = 500$ nm, and (d) $H_{MA} = 600$ nm.

metasurfaces for diverse applications, including multipolar Huygens metasurface,[48] directional scattering,[60] and superdirectivity.[61]

Lattice periodicity (P_{MS}) dictates coupling between Mie and lattice resonances

Metasurfaces, 2D lattice structures, are designed by placing each meta-atom, acting as the basis, at lattice sites, as shown in Fig. 3a.[62] Unlike the Mie resonance occurring at a wavelength $\lambda_{MA\text{-}Res}$ (=463 nm) corresponding to a meta-atom, interaction among each meta-atom resonance, depending on the lattice periodicity (P_{MS}), plays a crucial role in determining the resulting resonance, known as metasurface lattice resonance ($\lambda_{MS\text{-}Res}$), manifested as peaks in the EM spectra.[32,63] Interaction of light with a periodic lattice structure, not necessarily having Mie-resonant meta-atoms as the basis, results in an EM wave diffraction pattern, characterized by alternating maxima and minima, referred to as lattice resonances ($\lambda_{Lattice\text{-}Res}$) or diffraction orders in the light intensity pattern, whose angular positions can be accurately estimated by diffraction theory.[19] However, as an anomaly to the diffraction theory, rapid variations in the intensities of diffraction orders, known as the Rayleigh anomaly (RA), are observed in diffraction gratings, periodic lattice structures of both metals, as well as dielectrics.[19,36] The variations in the appearance of intensity maxima occur at Rayleigh anomaly (RA) wavelengths (λ_{RA}), which also depend on the lattice periodicity (P_{MS}) of the diffraction grating, including a crossed 2D grating, as in the case of metasurfaces.[19,36] For a metasurface (TiO_2) on an opaque substrate (Si), λ_{RA} depends not only on P_{MS}, but also on the effective refractive index of the metasurface (n_{eff}),[64] (eqn (8), SI), as given by the expression $\lambda_{RA} = n_{eff} \times P_{MS}$ and illustrated in Fig. 3d.

The role of P_{MS} in governing the interplay among different resonance types, (i) the meta-atom Mie resonance ($\lambda_{MA\text{-}Res}$),[30] (ii) metasurface lattice resonances ($\lambda_{MS\text{-}Res}$),[21,63] and (iii) the Rayleigh anomaly wavelength (λ_{RA}),[36] is investigated across three regimes of lattice periodicity (P_{MS}): (a) small ($P_{MS} < \lambda_{MA\text{-}Res}$), (b) intermediate ($P_{MS} \leq \lambda_{MA\text{-}Res}$), (c) comparable ($P_{MS} \sim \lambda_{MA\text{-}Res}$) and (d) large ($P_{MS} > \lambda_{MA\text{-}Res}$). The EM wave scattering cross-section (C_{sca}) is computed for a TiO_2 metasurface on a Si substrate as a function of wavelength (λ = 450–650 nm) for different lattice

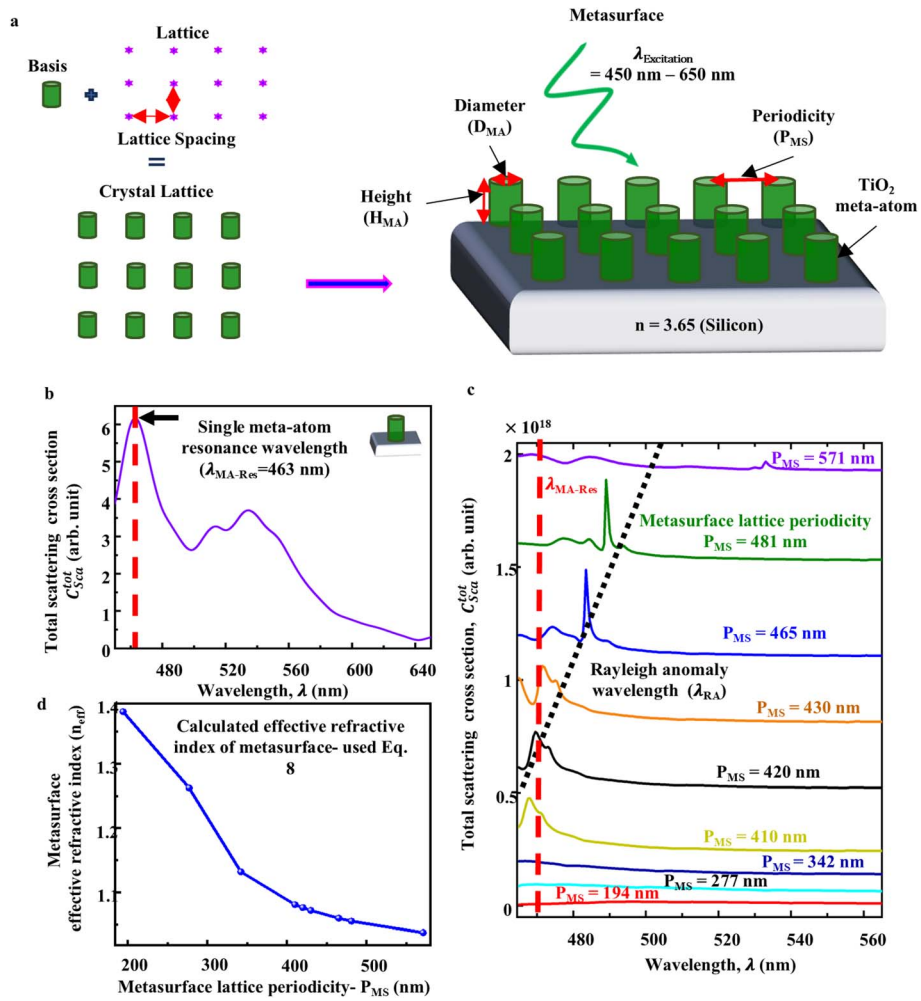

Fig. 3 (a) Schematic of a metasurface, (b) total scattering cross-section (C_{sca}) EM spectra of a meta-atom, (c) total scattering cross-section spectra across different metasurface lattice periodicities (P_{MS}), and (d) calculated effective refractive index of the metasurface (n_{eff}).

periodicities (P_{MS}) [Fig. 3c], considering the optimally designed resonant dimensions of a meta-atom in an air medium, obtained by numerical computation as discussed earlier. The meta-atom resonance wavelength ($\lambda_{MA\text{-}Res}$) is found to be 463 nm for the designed TiO_2 meta-atom on a Si substrate, with optimal dimensions (D_{MA} = 120 nm and H_{MA} = 600 nm), as shown in Fig. 3a. As the lattice periodicity (P_{MS}) increases from $P_{MS} < \lambda_{MA\text{-}Res}$ to $P_{MS} > \lambda_{MA\text{-}Res}$, three aspects are observed with regard to the resonance peak in the spectra: (a) a red shift towards longer wavelengths, (b) narrowing of the width and (c) shift towards λ_{RA} [Fig. 3b and c]. For the small periodicity regime, $P_{MS} < \lambda_{MA\text{-}Res}$ (P_{MS} = 194 nm, 222 nm, and 342 nm; $\lambda_{MA\text{-}Res}$ = 463 nm), no spectral peak is observed within the investigated wavelength range [Fig. 3c], as the probability of satisfying the resonance condition ($\lambda_{MS\text{-}Res} < 450$ nm) is higher at shorter wavelengths.[65] Moreover, the calculated values of λ_{RA} [Fig. 3c], being very low for small periodicity ($P_{MS} < \lambda_{MA\text{-}Res}$), do not fall within the investigated wavelength range. For the intermediate periodicity regime, $P_{MS} \leq \lambda_{MA\text{-}Res}$ (P_{MS} = 410 nm, 420 nm, and 430 nm; $\lambda_{MA\text{-}Res}$ = 463 nm), the observed spectral peaks ($\lambda_{MS\text{-}Res}$) are broad and lie at shorter wavelengths compared to the Rayleigh anomaly wavelength (λ_{RA}), *i.e.* $\lambda_{MS\text{-}Res} < \lambda_{RA}$ [Fig. 3c].[21,32,37,41,66] Metasurface lattice resonances ($\lambda_{MS\text{-}Res}$) originate from coupling, *i.e.* constructive interference of far–field interactions among meta-atom resonances ($\lambda_{MA\text{-}Res}$). However, the coupling is weak if the meta-atoms are in the vicinity of each other in the intermediate periodicity regime ($P_{MS} \leq \lambda_{MA\text{-}Res}$), leading to weak interference, which is manifested as the broad width of the observed lattice resonance spectral peaks, as shown in Fig. 3c. Moreover, the positions of the metasurface lattice resonance $\lambda_{MS\text{-}Res}$ are found to approach the corresponding λ_{RA} values with increase in P_{MS}. The $\lambda_{MS\text{-}Res}$ resonances are strongly coupled with ED, MD, and EQ, and these modes are called ED-LR, MD-LR, and EQ-LR, respectively (shown in Fig. S1 in the SI).

In the periodicity regime $P_{MS} \sim \lambda_{MA\text{-}Res}$ (P_{MS} = 465 nm and 481 nm), the optimum spacing between meta-atoms is achieved, and the spectral peak width becomes extremely narrow, which is attributed to collective resonances resulting from maximum coupling between two different natures of EM resonances: $\lambda_{MA\text{-}Res}$ and $\lambda_{Lattice\text{-}Res}$.[21,37,40,65] There is a strong enhancement from the ED-LR, MD-LR, and MQ-LR, as shown in Fig. 4. Interestingly, the spectral peak positions of the almost overlap with the respective λ_{RA} wavelength values [Fig. 3b and c]. The observation that $\lambda_{MS\text{-}Res}$ either overlaps with or lies in the proximity of the calculated λ_{RA} (dotted line) physically means that both meta-atom Mie resonance ($\lambda_{MA\text{-}Res}$) (dashed line) and P_{MS}-dependent lattice diffraction resonance makes equal contributions. Otherwise, the meta-atom Mie resonance ($\lambda_{MA\text{-}Res}$) primarily plays the key role. For the larger periodicity regime, $P_{MS} > \lambda_{MA\text{-}Res}$ (P_{MS} = 571 nm), *i.e.* for large separation among the meta-atoms, the spectral peak almost gets diminished, only showing a tiny amplitude, signifying a non-satisfied metasurface lattice resonance condition ($\lambda_{MS\text{-}Res}$), as shown in Fig. 3c.[19,40,65] This aspect is confirmed by the significant deviation of the weak spectral peak position ($\lambda_{MS\text{-}Res}$) from the λ_{RA} value, which means the necessary crossed-grating diffraction condition is not satisfied for such large values of lattice periodicity.[65] Therefore, for a given metasurface lattice structure on an opaque substrate, by tuning the lattice periodicity (P_{MS}) as a control parameter across different periodicity regimes, with respect to the single meta-atom resonance wavelength ($\lambda_{MA\text{-}Res}$) and the Rayleigh anomaly wavelength (λ_{RA}), the coupling among different natures of lattice resonances can be maximized, resulting in extremely strong metasurface lattice resonances $\lambda_{MS\text{-}Res}$, with extremely narrow widths, high magnitudes and large quality factors.[30]

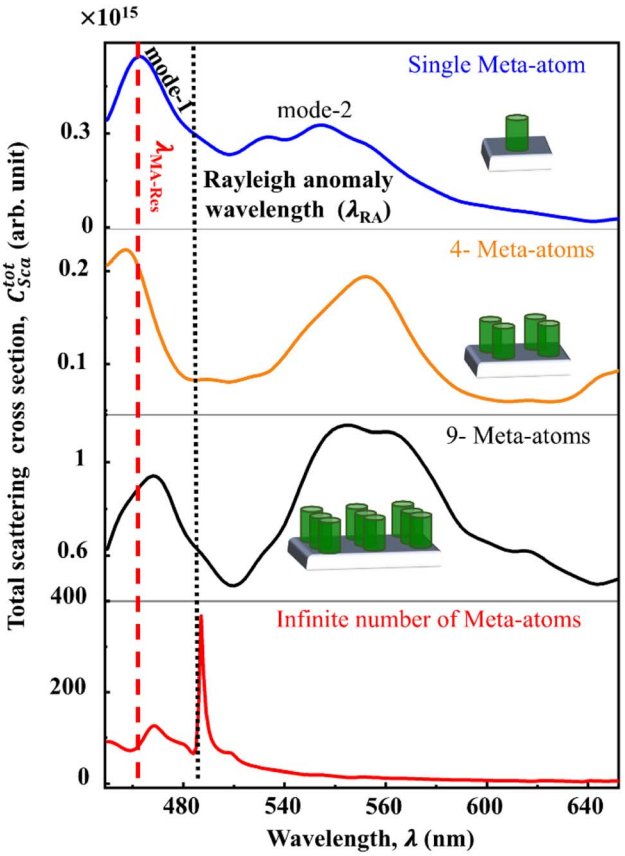

Fig. 4 Total scattering cross-section (C_{sca}) EM spectra of metasurfaces with different numbers of meta-atoms.

Number of meta-atoms in a finite metasurface dictates the spatial hybridization of EM multipoles

The computational simulations are, in general, performed by modelling only the unit cell of the array of meta-atoms and applying periodic boundary conditions, thereby modelling an infinite metasurface.[62] This approach significantly reduces the computational cost compared to modelling a finite array of individual meta-atoms. However, no array is infinite in real nanophotonic systems, and usually the size of the arrays that can be created is limited by the fabrication method.[43]

Considering real metasurfaces with a finite lattice array size, *i.e.*, a finite number of meta-atoms, computational simulations are compared for single, 4 (2 × 2), 9 (3 × 3) meta-atoms, and an

infinite metasurface. In order to design finite metasurfaces, the optimal geometric dimensions—the meta-atom height and diameter—in the periodicity regime ($P_{MS} \sim \lambda_{MA\text{-}Res} \sim 463$ nm) are considered, where maximum resonance, manifested as a sharp peak (narrow FWHM) and a high Q factor, is observed because of collective resonances ($\lambda_{MS\text{-}Res}$) resulting from maximum coupling between two different natures of EM resonances: $\lambda_{MA\text{-}Res}$ and $\lambda_{Lattice\text{-}Res}$, as discussed in the previous section [Fig. 3]. Although it is speculated that the strength of coupling, manifested as the resonance peak width, is dictated by the metasurface array size, *i.e.* the number of meta-atoms, a systematic investigation is still missing.

In this regard, the effect of increasing number of meta-atoms (N_{MA}) on the interplay among different metasurface resonance types, $\lambda_{MA\text{-}Res}$, $\lambda_{Lattice\text{-}Res}$, λ_{RA} and $\lambda_{MS\text{-}Res}$, are examined for $P_{MS} \sim \lambda_{MA\text{-}Res}$, as shown in Fig. 4. Two distinct collective metasurface resonance modes ($\lambda_{MS\text{-}Res}$), designated as mode-1 and mode-2, are observed with an increasing number of meta-atoms (N_{MA}) while spatially arranged in a symmetric manner. In the case of a single meta-atom (Fig. 4), mode-1 ($\lambda_{MA\text{-}Res\text{-}mode\text{-}1}$) appears significantly stronger than mode-2 ($\lambda_{MA\text{-}Res\text{-}mode\text{-}2}$). In order to get a better idea about the contribution of multipole nature (electric or magnetic) and order (dipole or quadrupole) to the total scattering cross-section (C_{sca}^{total}), scattering cross-section for each multipole (ED, MD, EQ, and MQ) is computed (Fig. S2, SI). All four multipoles significantly contribute to the resultant resonance mode-1 (shown in Fig. S2, SI), whereas mode-2 is primarily supported by the MD and EQ, with less contributions from the ED and MQ. As per the phase symmetry of EM multipoles, ED and MQ are of even parity, while MD and EQ are of odd parity.[44,67] Hence, for a single meta-atom, mode-2 is primarily governed by multipoles of the same parity, with different nature and order. As the number of meta-atoms increases ($N_{MS} = 4$; 2×2), while satisfying the optimal periodicity regime condition, $P_{MS} \sim \lambda_{MA\text{-}Res}$, the amplitude of resonance mode-2 becomes comparable to that of resonance mode-1. The lower-order multipoles of different nature (ED and MD) and parity make the major contribution to mode-1. Multipoles, ED and MQ, with different nature and order, however, with the same parity, primarily contribute to mode-2 (shown in Fig. S2, SI).[44,67]

On further increasing the number of meta-atoms (3×3), the amplitude of resonance mode-2 surpasses that of mode-1, as shown in Fig. 4. EM multipoles (ED, EQ and MQ) with different nature, order, and parity, except MD, contribute to resonance mode-1.[44,67] However, all four multipoles make equal and significant contributions to mode-2, leading to its amplitude surpassing that of mode-1. Therefore, as the number of meta-atoms increases ($1 \rightarrow 9$), the following aspects are found to be noteworthy: (i) resonance mode-1, where the $\lambda_{MA\text{-}Res}$ makes a small red shift towards the λ_{RA} position; and (ii) the resonance mode-2, where the $\lambda_{MS\text{-}Res}$, resulting from coupling between $\lambda_{MA\text{-}Res}$ and $\lambda_{Lattice\text{-}Res}$, makes a large blue shift towards the λ_{RA} position, signifying the influence of lattice periodicity on collective metasurface lattice resonances ($\lambda_{MS\text{-}Res}$) with increasing numbers of meta-atoms.[44,67] In the case of an infinite metasurface ($N_{MS} = \infty$), modeling infinite number of meta-atoms by applying periodic boundary conditions as discussed in Fig. 3c, resonance mode-1 almost gets diminished, while resonance mode-2 becomes dominant, having an extremely narrow peak width and high amplitude, indicating the emergence of a high-Q-factor resonance [Fig. 3c and 5].[44,68,70] Interestingly, the wavelength position of the resonance mode-2 ($\lambda_{MS\text{-}Res}$) exactly overlaps with the λ_{RA} position if the optimal periodicity regime condition $P_{MS} \sim \lambda_{MA\text{-}Res}$ is satisfied for the infinite metasurface. The

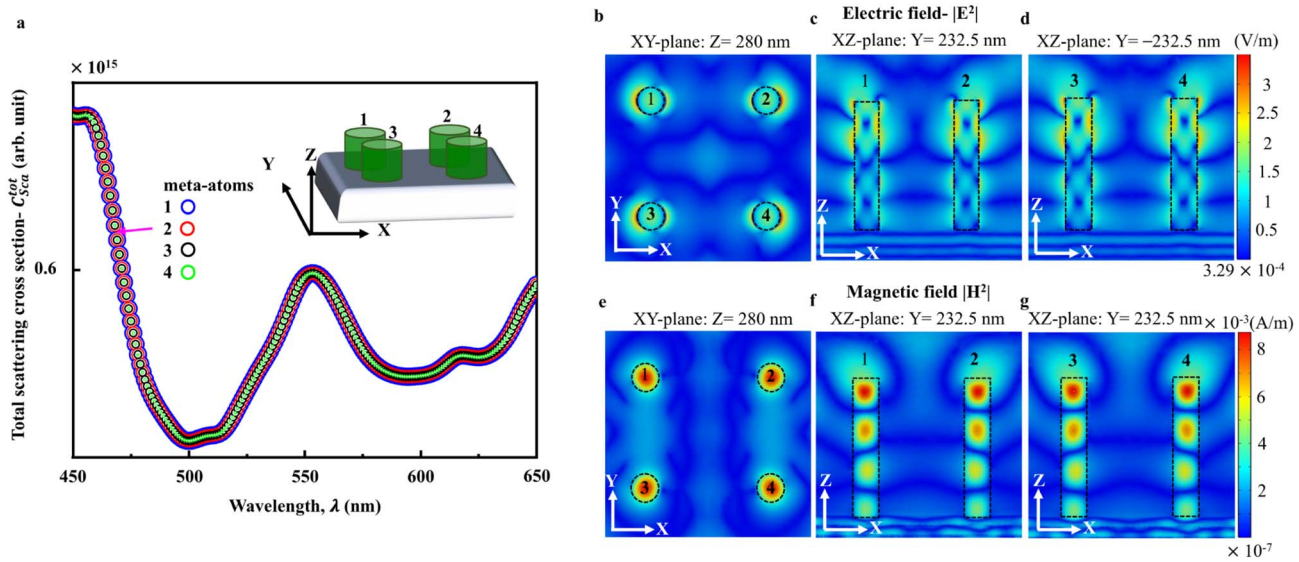

Fig. 5 (a) Total scattering cross-section (C_{sca}) EM spectrum of 4 (2×2) meta-atom unit cell; electric field distributions: (b) *XY* plane, $Z = 280$ nm; (c) *XZ* plane, $Y = 232.5$ nm; and (d) *XZ* plane, $Y = -232.5$ nm; and magnetic field distribution: (e) *XY* plane, $Z = 280$ nm; (f) *XZ* plane, $Y = 232.5$ nm; and (g) *XZ* plane, $Y = -232.5$ nm.

three multipoles (ED, MD and MQ) are found to make major contributions to resonance mode-2, with hardly any contribution from the EQ.[37,47]

Local EM field distribution is influenced by spatial hybridization of EM multipoles corresponding to neighboring meta-atoms

In addition to the knowledge of finite meta-atom metasurfaces at a global scale, understanding the total scattering cross-section (C_{sca}^{total}) and field distributions (electric $|E|^2$ and magnetic $|H|^2$) at the local meta-atom scale is crucial for different applications, including quantum emitters,[49] Raman signal enhancement,[50] low-threshold nano-lasers,[51] and other cavity-free integrated resonant photonic circuit devices.[52] It is to be noted that while designing finite metasurfaces (TiO_2 on Si substrate) with different numbers of meta-atoms (2 × 2 and 3 × 3), optimal geometric dimensions, including the meta-atom height, diameter and lattice periodicity ($P_{MS} \sim \lambda_{MA\text{-}Res}$), are considered, where metasurface resonances ($\lambda_{MA\text{-}Res}$), manifested as narrow spectral peak widths (FWHM) with high quality (Q) factor, are observed.[44,68,70]

In the case of a finite metasurface with 2 × 2 meta-atoms, C_{sca}^{total}, considering multipoles (ED, MD, EQ and MQ) of different order and nature for each meta-atom (indices 1, 2, 3 and 4), is found to overlap exactly with each other, as shown in Fig. 5. Both the electric as well as magnetic fields show asymmetric distributions, where the field strengths $|E|^2$ and $|H|^2$ are higher for each meta-atom in the direction of its outer periphery that lacks a neighboring meta-atom, as observed in both the horizontal cross-sectional (XY plane, $Z = 280$ nm) and vertical cross-sectional (XZ plane, $Y = 232.5$ and -232.5 nm) planes. The periodicity regime $P_{MS} \sim \lambda_{MA\text{-}Res}$, *i.e.* the separation distance between two neighboring meta-atoms (P_{MS}), is comparable to the single meta-atom resonance wavelength ($\lambda_{MA\text{-}Res}$), is found to be optimal for maximum strength mode coupling with neighboring meta-atom field distribution, known as spatial hybridization, resulting in a strong local field in the meta-atom of interest.[69–71] This leads to the redistribution of the fields of each meta-atom towards the outer periphery in the direction away from the neighboring meta-

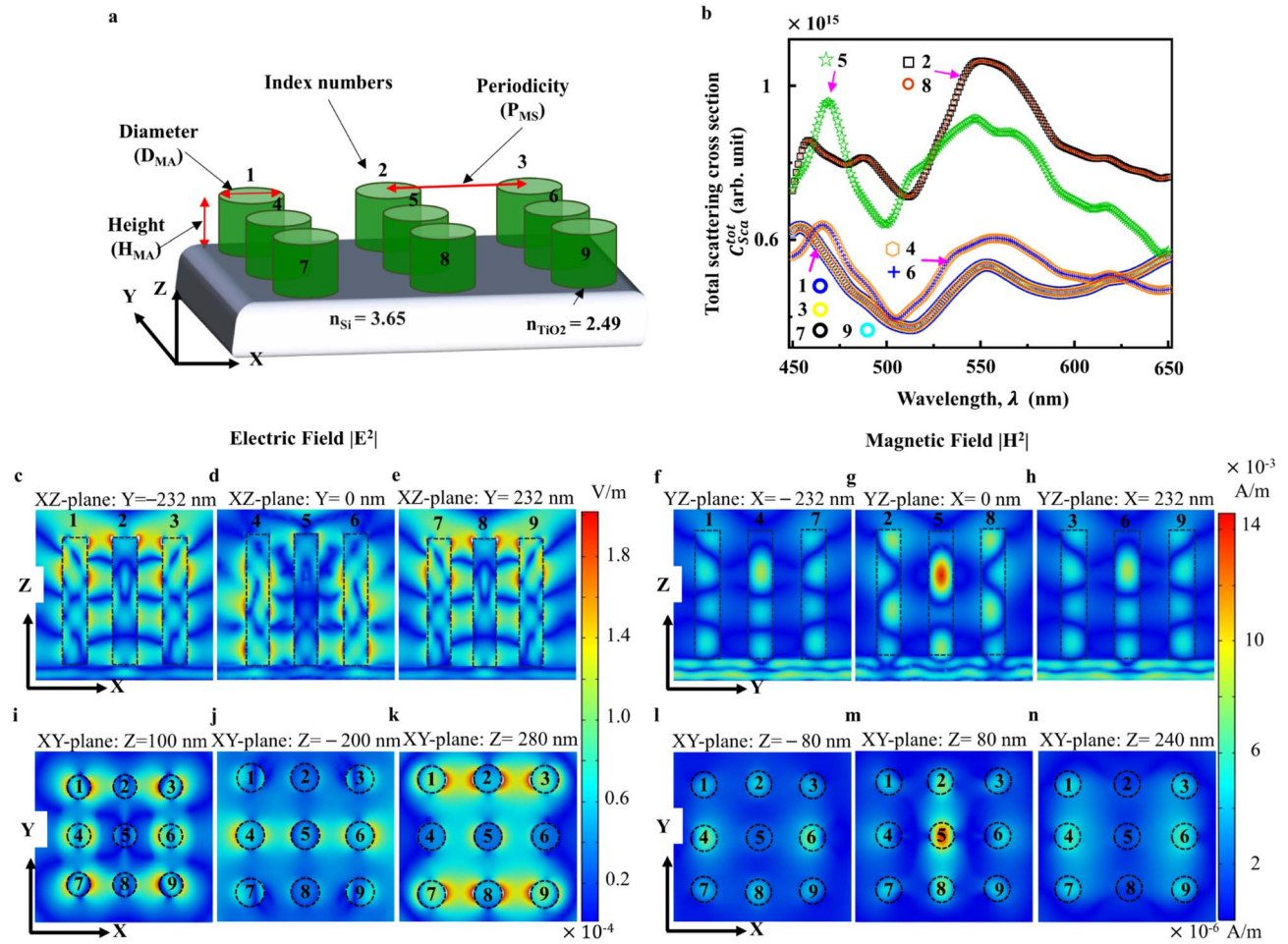

Fig. 6 (a) Schematic of a metasurface containing 9 (3 × 3) meta-atoms; (b) total scattering cross-section (C_{sca}) EM spectra; electric field distributions: (c) XZ plane, $Y = 233.5$ nm; (d) XZ plane, $Y = 0$ nm; (e) XZ plane, $Y = -232.5$ nm, (i) XY plane, $Z = 100$ nm, (j) XY plane, $Z = -200$ nm; and (k) XY plane, $Z = 280$ nm; and magnetic field distributions: (f) YZ plane, $X = -233.5$ nm; (g) YZ plane, $X = 0$ nm; (h) YZ plane, $X = 232.5$ nm; (l) XY plane, $Z = -80$ nm; (m) XY plane, $Z = 80$ nm; and (n) XY plane, $Z = 240$ nm.

atoms, as shown in Fig. 5b and c. The directionality and degree of spatial hybridization, manifested as the overlap of field lobes, are observed for both electric and magnetic fields.

The asymmetry and inhomogeneity in the field distribution of each meta-atom are retained even when the number of meta-atoms is increased to 9 (3×3). The meta-atom (index-5), located in the centre of the metasurface, shows maximum localization of EM fields under the optimal periodicity regime $P_{MS} \sim \lambda_{MA\text{-}Res} \sim 465$ nm due to spatial hybridization with the fields of neighbouring meta-atoms across all directions, which is reflected as the field-lobe overlap in $|H|^2$, as shown in Fig. 6g and m. This is reason for the total scattering cross-section (C_{sca}^{total}) of the meta-atom (index-5) is also found to be maximum (Fig. 6b).[72,73] The scattering cross-section as well as field distributions of each meta-atom, except the symmetrically surrounded centre one (index-5), are found to be different (Fig. 6) due to spatial hybridization with asymmetrically arranged neighbouring meta-atoms.

Conclusion

In conclusion, we have developed a bottom-up, comprehensive design framework for all-dielectric metasurfaces to maximize resonance strength, as manifested through enhanced scattering cross-sections and local field distributions by controlled excitation and overlap of multipoles, leading to controlled coupling among different resonance types—Mie resonance, lattice resonance, Rayleigh anomaly—by tuning geometric dimensions, such as height, diameter, lattice periodicity and number of meta-atoms as the control parameters, based on finite element method (FEM) numerical simulations. Spectral overlap of all four resonantly excited multipoles is demonstrated for a meta-atom when the height is increased beyond the excitation wavelength. The lattice periodicity plays a key role in determining the Q factor and spectral position of collective metasurface resonances across different periodicity regimes with regard to the Mie resonance wavelength. Two noteworthy aspects are found for the meta-atom spacing in the lattice periodicity regime ($P_{MS} \sim \lambda_{MA\text{-}Res}$). First, a high Q-factor is realized in the lattice periodicity regime ($P_{MS} \sim \lambda_{MA\text{-}Res}$), originating from maximum coupling of resonantly excited meta-atom multipole-induced Mie resonances ($\lambda_{MA\text{-}Res}$) with lattice resonances ($\lambda_{LS\text{-}Res}$). Second, the resulting metasurface resonance wavelength ($\lambda_{MS\text{-}Res}$) exactly coincides with the Rayleigh anomaly wavelength (λ_{RA}), which signifies maximum contribution from both (a) lattice periodicity-controlled diffraction lattice resonances and (b) coupling of meta-atom Mie resonances with lattice resonances. However, for other lattice periodicity regimes ($P_{MS} < \lambda_{MA\text{-}Res}$ and $P_{MS} > \lambda_{MA\text{-}Res}$), the coupling is found to be weak, leading to a decreased Q-factor. In real-world metasurfaces consisting of a finite number of meta-atoms, the spatial hybridization of EM field occurs due to the specific spatial arrangement of neighboring meta-atoms, which depends on the array size, as manifested in the spectral resonance peak position tuning and local field asymmetry at the sub-meta-atom scale. Overall, the insights we presented not only enhance the basic understanding of multipole enhancement, overlap, and coupling among different resonance types, but also paves the way for the practical design of metasurface photonic platforms with tailored light–matter interactions, applicable in areas including photonic quantum devices and resonant waveguide gratings.

Conflicts of interest

The authors declare that they have no conflict of interest.

Data availability

The data supporting this article included in the main text are available at: https://drive.google.com/drive/folders/13OUCORgHo236XvEw4vipYQrc-zXkkSHk?usp=drive_link.

Supplementary information (SI): the theoretical background of the scattering cross-section multipole equations as well as the effective refractive index of metasurface on opaque substrate. In addition, the file includes the scattering cross-sections corresponding to different electromagnetic multipoles (ED, MD, EQ, and MQ) for (i) varying lattice periodicity, which supports Fig. 3b in the main article, and (ii) varying number of meta-atoms in the infinite metasurface, which supports Fig. 4 in the main article. See DOI: https://doi.org/10.1039/d6na00100a.

Acknowledgements

The author T. K. B. gratefully acknowledges the SRM Institute of Science and Technology, Kattankulathur, Chennai, India, for providing PhD fellowship. T. K. B. and J. M. L. express their sincere gratitude to Prof. Prabhakar Subrahmanyam, Prof. B. K. Gnanavel, and Dr Manikandan S for providing high-performance computing facilities at the Center of Excellence for Electronic Cooling and Computational Fluid Dynamics (CFD), Department of Physics and Nanotechnology for High-Performance Computing Center (HPCC) at the SRM Institute of Science and Technology, Kattankulathur, Chennai, India.

References

1 Z. A. Arnon, D. Pinotsi, M. Schmidt and S. Gilead, *ACS Appl. Mater. Interfaces*, 2019, **10**, 20783–20789.
2 A. E. Seago, P. Brady, J. P. Vigneron and T. D. Schultz, *J. R. Soc. Interface*, 2009, **6**, S165–S184.
3 S. Kinoshita, S. Yoshioka and K. Kawagoe, *Proc. R. Soc. B*, 2002, **269**, 1417–1421.
4 A. González-Tudela, A. Reiserer and J. J. García-Ripoll, *Nat. Rev. Phys.*, 2024, **3**, 166–179.
5 S. Jahani and Z. Jacob, *Nat. Nanotechnol.*, 2016, **11**, 23–36.
6 M. Shehbaz, C. Du, D. Zhou, S. Xia and Z. Xu, *Applied Physics Reviews*, 2023, **10**, 1–45.
7 N. Meinzer, W. L. Barnes and I. R. Hooper, *Nat. Photonics*, 2014, **8**, 889–898.
8 D. A. Powell, *Phys. Rev. B: Condens. Matter Mater. Phys.*, 2014, **90**, 1–10.
9 M. V. Rybin and Y. Kivshar, *npj Nanophotonics*, 2024, **1**, 43.
10 Y. Tamayama and K. Kanari, *Phys. Rev. B*, 2020, **102**, 1–10.

11 W. Bogaerts, P. de Heyn, T. van Vaerenbergh, K. de Vos, S. Kumar Selvaraja, T. Claes, P. Dumon, P. Bienstman, D. van Thourhout and R. Baets, *Laser Photonics Rev.*, 2012, **6**, 47–73.
12 A. Chiasera, Y. Dumeige, P. Féron, M. Ferrari, Y. Jestin, G. N. Conti, S. Pelli, S. Soria and G. C. Righini, *Laser Photonics Rev.*, 2010, **4**, 457–482.
13 J. D. Joannopoulos, P. R. Villeneuve and S. Fan, *Nature*, 1997, **386**, 143–149.
14 Y. Kivshar, *Nano Lett.*, 2022, **22**, 3513–3515.
15 V. E. Babicheva and A. B. Evlyukhin, *Adv. Opt. Photonics*, 2023, **16**, 539–658.
16 A. Vaskin, R. Kolkowski, A. F. Koenderink and I. Staude, *Nanophotonics*, 2019, **8**, 1151–1198.
17 Y. L. Tang, T. H. Yen, K. Nishida, C. H. Li, Y. C. Chen, T. Zhang, C. K. Pai, K. P. Chen, X. Li, J. Takahara and S. W. Chu, *Nat. Commun.*, 2023, **14**, 1–8.
18 L. Huang, R. Jin, C. Zhou, G. Li, L. Xu, A. Overvig, F. Deng, X. Chen, W. Lu, A. Alù and A. E. Miroshnichenko, *Nat. Commun.*, 2023, **14**, 1–9.
19 G. Quaranta, G. Basset, O. J. F. Martin and B. Gallinet, *Laser Photonics Rev.*, 2018, **12**, 1–31.
20 M. F. Limonov, M. V. Rybin, A. N. Poddubny and Y. S. Kivshar, *Nat. Photonics*, 2017, **11**, 543–554.
21 S. Tsoi, F. J. Bezares, A. Giles, J. P. Long, O. J. Glembocki, J. D. Caldwell and J. Owrutsky, *Appl. Phys. Lett.*, 2016, **108**, 111101.
22 S. Baur, S. Sanders and A. Manjavacas, *ACS Nano*, 2018, **12**, 1618–1629.
23 S. Shen, Z. Ruan, S. Li, Y. Yuan and H. Tan, *Results Phys.*, 2021, **23**, 104057.
24 H. Radhakrishnan, T. K. Basha, J. M. Laskar, G. Krishnan, S. Dhara and R. Pandian, *ACS Photonics*, 2025, **12**, 4503–4511.
25 C. W. Hsu, B. Zhen, A. D. Stone, J. D. Joannopoulos and M. Soljacic, *Nat. Rev. Mater.*, 2016, **1**, 16048.
26 T. Liu, R. Xu, P. Yu, Z. Wang and J. Takahara, *Nanophotonics*, 2020, **9**, 1115–1137.
27 J. M. Laskar, J. Philip and B. Raj, *Phys. Rev. E: Stat., Nonlinear, Soft Matter Phys.*, 2008, **78**, 1–9.
28 V. Zubyuk, L. Carletti, M. Shcherbakov and S. Kruk, *APL Mater.*, 2021, **9**, 060701.
29 S. A. Schulz, *et al.*, *Appl. Phys. Lett.*, 2024, **124**, 1–114.
30 Z. Zhang, P. Liu, W. Lu, P. Bai, B. Zhang, Z. Chen, S. A. Maier, J. Gómez Rivas, S. Wang and X. Li, *Fundam. Res.*, 2023, **3**, 822–830.
31 G. W. Castellanos, P. Bai and J. Gómez Rivas, *J. Appl. Phys.*, 2019, **125**, 213105.
32 V. E. Babicheva and J. V. Moloney, *Nanophotonics*, 2018, **7**, 1663–1668.
33 V. I. Zakomirnyi, A. E. Ershov, V. S. Gerasimov, S. V. Karpov, H. Ågren and I. L. Rasskazov, *Opt. Lett.*, 2019, **44**, 5743.
34 C. H. Palmer and F. C. Evering, *J. Opt. Soc. Am.*, 1964, **54**, 844.
35 R. W. Wood, *Proc. Phys. Soc., London*, 1901, **18**, 269–275.
36 L. Rayleigh, *Proc. R. Soc. London*, 1907, **79**, 399–416.
37 V. E. Babicheva and A. B. Evlyukhin, *Laser Photonics Rev.*, 2017, **11**, 1–10.
38 A. Han, C. Dineen, V. E. Babicheva and J. V. Moloney, *Nanophotonics*, 2020, **9**, 3545–3556.
39 R. Xu and J. Takahara, *Opt. Lett.*, 2021, **46**, 3596.
40 C. Liu, H. Ye, Y. Wang, Y. Sun, Y. Liu, Z. Yu and L. Yu, *Opt. Lett.*, 2020, **45**, 4847.
41 V. E. Babicheva and A. B. Evlyukhin, *ACS Photonics*, 2018, **5**, 2022–2033.
42 K. Sakai, K. Nomura, T. Yamamoto, T. Omura and K. Sasaki, *Sci. Rep.*, 2016, **6**, 1–7.
43 D. Hähnel, C. Golla, M. Albert, T. Zentgraf, V. Myroshnychenko, J. Förstner and C. Meier, *Light: Sci. Appl.*, 2023, **12**, 23–26.
44 T. X. Hoang, D. Leykam, H. S. Chu, C. E. Png, F. J. García-Vidal and Y. S. Kivshar, *Phys. Rev. Res.*, 2025, **7**, 13316.
45 E. N. Bulgakov and A. F. Sadreev, *Phys. Rev. A*, 2019, **3**, 033851.
46 Z. Liu, Y. Xu, Y. Lin, J. Xiang, T. Feng, Q. Cao, J. Li, S. Lan and J. Liu, *Phys. Rev. Lett.*, 2019, **123**, 1–6.
47 V. Karimi and V. E. Babicheva, *Opt. Express*, 2023, **31**, 16857.
48 S. Liu, A. Vaskin, S. Campione, O. Wolf, M. B. Sinclair, J. Reno, G. A. Keeler, I. Staude and I. Brener, *Nano Lett.*, 2017, **17**, 4297–4303.
49 J. Ma, J. Zhang, J. Horder, A. A. Sukhorukov, M. Toth, D. N. Neshev and I. Aharonovich, *Adv. Mater.*, 2024, **36**, 1–15.
50 S. Izadshenas and K. Słowik, *APL Mater.*, 2023, **11**, 1–9.
51 T. C. Ellis, S. Eslami and S. Palomba, *Nanophotonics*, 2024, **13**, 2707–2739.
52 L. Huang, L. Xu, M. Woolley and A. E. Miroshnichenko, *Adv. Quantum Technol.*, 2020, **3**, 1900126.
53 J. R. DeVore, *J. Opt. Soc. Am.*, 1951, **41**, 416.
54 D. E. Aspnes and A. A. Studna, *Phys. Rev. B: Condens. Matter Mater. Phys.*, 1983, **27**, 985–1009.
55 R. Alaee, C. Rockstuhl and I. Fernandez-Corbaton, *Opt. Commun.*, 2018, **407**, 17–21.
56 M. V. Rybin, K. L. Koshelev, Z. F. Sadrieva, K. B. Samusev, A. A. Bogdanov, M. F. Limonov and Y. S. Kivshar, *Phys. Rev. Lett.*, 2017, **119**, 1–5.
57 I. Staude, A. E. Miroshnichenko, M. Decker, N. T. Fofang, S. Liu, E. Gonzales, J. Dominguez, T. S. Luk, D. N. Neshev, I. Brener and Y. Kivshar, *ACS Nano*, 2013, **7**, 7824–7832.
58 J. van de Groep and A. Polman, *Opt. Express*, 2013, **21**, 26285.
59 C. Liu, L. Chen, T. Wu, Y. Liu, R. Ma, J. Li, Z. Yu, H. Ye and L. Yu, *New J. Phys.*, 2020, **22**, 023018.
60 R. Alaee, R. Filter, D. Lehr, F. Lederer and C. Rockstuhl, *Opt. Lett.*, 2015, **40**, 2645.
61 A. Radkovskaya, S. Kiriushechkina, A. Vakulenko, P. Petrov, L. Solymar, L. Li, A. Vallecchi, C. J. Stevens and E. Shamonina, *J. Appl. Phys.*, 2018, **124**, 104901.
62 J. Hou, X. Zhang, Y. Guo, R. Z. Zhang and M. Guo, *Sci. Rep.*, 2023, **13**, 1–7.
63 V. E. Babicheva and A. B. Evlyukhin, *J. Appl. Phys.*, 2021, **129**, 040402.
64 D. Visser, D. Y. Chen, Y. Désières, A. P. Ravishankar and S. Anand, *Sci. Rep.*, 2020, **10**, 12527.
65 F. J. G. De Abajo, *Rev. Mod. Phys.*, 2007, **79**, 1267–1290.

66 M. Decker, I. Staude, M. Falkner, J. Dominguez, D. N. Neshev, I. Brener, T. Pertsch and Y. S. Kivshar, *Adv. Opt. Mater.*, 2015, **3**, 813–820.
67 W. Liu and Y. S. Kivshar, *Opt. Express*, 2018, **26**, 13085.
68 S. Izadshenas and K. Słowik, *APL Mater.*, 2023, **11**, 081120.
69 S. Sehrawat, R. Kolkowski and A. Shevchenko, *New J. Phys.*, 2024, **26**, 23050.
70 I. Allayarov, A. B. Evlyukhin and A. Calà Lesina, *Opt. Express*, 2024, **32**, 5641.
71 M. Pascale, G. Miano, R. Tricarico and C. Forestiere, *Sci. Rep.*, 2019, **9**, 1–21.
72 Y. Guo, Y. Liao, Y. Yu, Y. Shi and S. Xiong, *Opt. Lett.*, 2020, **45**, 5604.
73 N. Ustimenko, C. Rockstuhl and A. B. Evlyukhin, *Phys. Rev. B*, 2024, **109**, 1–14.